Article

# Snapshots of the catalytic cycle of an O2, pyridoxal phosphate-dependent hydroxylase

Jason B. Hedges, Eugene Kuatsjah, Yi-Ling Du, Lindsay D. Eltis, and Katherine S Ryan

*ACS Chem. Biol.*, **Just Accepted Manuscript** • DOI: 10.1021/acschembio.8b00039 • Publication Date (Web): 21 Feb 2018



ACS Publications

ACS Chemical Biology is published by the American Chemical Society. 1155 Sixteenth Street N.W., Washington, DC 20036

# Snapshots of the catalytic cycle of an $O_2$, pyridoxal phosphate-dependent hydroxylase

**Authors**

Jason B. Hedges,[1] Eugene Kuatsjah,[2] Yi-Ling Du,[4] Lindsay D. Eltis,[3] Katherine S. Ryan[1*]

**Author Affiliations**

[1]Department of Chemistry, [2]Genome Science and Technology Program, and [3]Department of Microbiology and Immunology, The University of British Columbia, Vancouver, British Columbia, Canada.

[4]Institute of Pharmaceutical Biotechnology, School of Medicine, Zhejiang University, Hangzhou, China

[*]Correspondence: ksryan@chem.ubc.ca

**ABSTRACT**

Enzymes that catalyze hydroxylation of unactivated carbons normally contain heme- and non-heme iron cofactors. By contrast, how a pyridoxal phosphate (PLP)-dependent enzyme could catalyze such a hydroxylation was unknown. Here, we investigate RohP, a PLP-dependent enzyme that converts L-arginine to (*S*)-4-hydroxy-2-ketoarginine. We determine that the RohP reaction consumes oxygen, with stoichiometric release of $H_2O_2$. To understand this unusual chemistry, we obtain ~1.5 Å resolution structures that capture intermediates along the catalytic cycle. Our data suggest that RohP carries out a four-electron oxidation and a stereospecific alkene hydration to give the (*S*)-configured product. Together with our earlier studies on an $O_2$, PLP-dependent L-arginine oxidase, our work suggests that there is a shared pathway leading to both oxidized and hydroxylated products from L-arginine.

## INTRODUCTION

Activation of carbon-hydrogen (C-H) bonds on $sp^3$-hybridized carbons is an enduring challenge in chemical synthesis.[1,2] Metalloenzymes, nature's solution to this challenge, have evolved the incredible capacity to catalyze the stereospecific functionalization of C-H bonds under mild conditions. Common cofactors for such enzyme-catalyzed reactions are heme and non-heme irons. For example, in the case of hydroxylation of L-arginine, the Fe(II)-, α-ketoglutarate-dependent enzymes VioC, YcfD, and OrfP catalyze hydroxylations of the $sp^3$-hybridized carbons of the L-arginine side chain.[3–5] By contrast, organic cofactors such as pyridoxal phosphate (PLP) are not normally expected to catalyze installation of hydroxyl groups onto unactivated $sp^3$-hybridized carbons.

PLP is one of the most widely used cofactors for enzymatic manipulation of amino acid substrates.[6] In the course of catalysis, many PLP-dependent enzymes form a carbanionic intermediate, called a quinonoid, which can result from deprotonation or decarboxylation of an amino acid-PLP adduct.[7] Normally, this quinonoid intermediate is sequestered in the active site of the enzyme and thus protected from reaction with $O_2$. However, in several cases this quinonoid intermediate can be subject to off-pathway reactions with electrophiles, including $O_2$.[8] The $O_2$-dependent oxidative deamination catalyzed by DOPA decarboxylase[9] and the $O_2$-dependent oxidative decarboxylation catalyzed by ornithine decarboxylase[10] are two well-characterized examples of such paracatalytic enzymatic activities. More recently, the diversity of PLP-dependent enzymes has expanded with the discovery of enzymes that use $O_2$ as a co-substrate to perform their primary enzymatic activities. For example, both petunia phenylacetaldehyde synthase and the celesticetin biosynthetic enzyme CcbF catalyze $O_2$-, PLP-dependent decarboxylation-coupled oxidative deaminations,[11,12] and Cap15 is an $O_2$-, PLP-dependent monooxygenase-decarboxylase that generates uridine-5'-carboxamide on the pathway to capuramycin.[13]

Intriguingly, the scope of such $O_2$-, PLP-dependent reactions is not limited to oxidative decarboxylations but also includes functionalization of unactivated C-H bonds. In 1977, Eguchi and coworkers purified an active fraction from *Streptomyces eurocidicus* SF 506 that could convert L-arginine to 2-ketoarginine and 4-hydroxy-2-ketoarginine using PLP and $O_2$.[14] This work tantalizingly suggested that a PLP-dependent enzyme

could use $O_2$ to catalyze a reaction that resulted in hydroxylation of an unactivated carbon center. However, the identity of the enzyme, the configuration of its product, and its likely mechanism involved remained unknown. More recently, Silvaggi and coworkers revealed that the fold-type I PLP-dependent enzyme MppP is responsible for production of 2-ketoarginine (**2**) and 4-hydroxy-2-ketoarginine (**4**, configuration unknown) from L-arginine on the pathway to the non-proteinogenic amino acid L-enduracididine, a precursor to the antibiotic mannopeptimycin.[15] They demonstrated that MppP consumes $O_2$, suggesting that this enzyme has evolved the ability to activate $O_2$ for a challenging hydroxylation reaction. They also solved two crystal structures of MppP. One of these structures shows PLP bound as an internal aldimine to Lys221, and the second structure has D-arginine, which is not a substrate, bound in an external aldimine with PLP. However, the N-terminus is disordered and the active site is exposed to solvent in all but one chain of the holo-enzyme, where it forms a small α-helix that points away from the active site and into the solvent. The lack of a closed active site and the lack of structures with native substrates bound in the active site raise questions about how catalysis might proceed past formation of the external aldimine. Furthermore, the specific role of oxygen in this reaction remains unknown.

In our group, we discovered a predicted fold-type I PLP-dependent enzyme Ind4 from the indolmycin biosynthetic pathway.[16,17] This enzyme, like MppP, catalyzes the two-electron oxidation of L-arginine to give 2-ketoarginine (**2**) (Figure 1). But, unlike MppP, Ind4 also catalyzes the four-electron oxidation of L-arginine to give didehydroarginine (2-amino-5-guanidinopenta-2,4-dienoate, **8a**) (Figure S1). The imine tautomer (**8b**) of this product can be intercepted by the downstream enzyme Ind5 for a stereospecific NADH-dependent reduction to give D-dehydroarginine (**9**) (Figure S1). In the absence of Ind5, the imine tautomer is hydrolyzed to compound **6**, which reacts with $H_2O_2$ released from the reaction to give compound **7** (Figure 1). As we unraveled this enzymology, we were curious whether enzymes similar to Ind4 are more widely distributed in natural product pathways, and we identified a putative biosynthetic gene cluster encoding an Ind4 homolog. Here, we report our discovery and characterization of the new Ind4 homolog, which we name RohP, and we demonstrate that it catalyzes an MppP-like reaction. To provide a mechanistic framework for understanding how RohP

catalyzes a hydroxylation – instead of an Ind4-like oxidation – we carry out extensive mass spectral, kinetic, stoichiometric, and X-ray crystallographic experiments. Our work suggests that both the RohP hydroxylase and the Ind4 oxidase catalyze challenging reactions of L-arginine through similar oxidative pathways. In particular, our crystallographic and stoichiometric studies support a mechanism where both the oxidase and hydroxylase carry out an $O_2$-dependent four-electron oxidation on L-arginine, giving a PLP-tethered didehydroarginine. Whereas Ind4 then releases didehydroarginine as a product, RohP additionally catalyzes a stereospecific alkene hydration on the PLP-tethered didehydroarginine, using water to give the hydroxylated product.

## RESULTS AND DISCUSSION

**RohP is an L-arginine hydroxylase** In our previous work, we discovered the $O_2$-, PLP-dependent oxidase Ind4, which generates the conjugated didehydroarginine (**8a**) from L-arginine (**1**) (Figure S1). We were curious whether similar enzymes are found in other bacteria. Using BLAST-P to search for similar enzymes in other bacteria, we identified an enzyme (accession number: AEW92768.1) from *Streptomyces cattleya* NRRL 8057 with 43% sequence identity to Ind4,[17] 40% sequence identity to the Ind4-like enzyme Pel4,[17] 32% sequence identity to MppP,[15] and 31% sequence identity to the MppP-like enzyme EndP (Figure S2).[18] This newly identified enzyme is encoded in a putative biosynthetic gene cluster unrelated to the indolmycin, mannopeptimycin, or other characterized gene clusters, and the function corresponding to this cluster is unknown (Figure S3). This close sequence identity of the encoded enzyme to both Ind4 and MppP suggests that it could have either Ind4-like or MppP-like activity, or perhaps catalyze a different reaction on L-arginine. As a first step in elucidating the product of this gene cluster, we determined the function of this enzyme. Based on the sequencing data, this enzyme is annotated with ~20 amino acid truncation in the N-terminus when compared to the other, characterized enzymes (Figure S2). We purified the recombinant enzyme from *E. coli* and tested whether it is also active on L-arginine. However, we found that the enzyme was inactive on L-arginine as purified or with exogenous PLP (Figure S4A). After determining that the enzyme was inactive with L-arginine, we re-sequenced the upstream region of DNA from *S. cattleya,* and we observed that one cytosine was missing

from the deposited sequence. With the correct number of cytosines, an alternate annotation of the gene would have a different start site and encode an enzyme 25 amino acids longer that aligns along the full length of MppP, Ind4, and the other characterized enzymes (Figure S2).

We recloned the gene including the new start site into pET28a, purified the enzyme from *E. coli*, and assayed the enzyme with L-arginine. After 16 h of incubation, we derivatized the reaction with dansyl chloride and analyzed it by HPLC. This experiment revealed that the L-arginine was consumed in the overnight assay (Figure S4B), suggesting that the enzyme – like Ind4, Pel4, and MppP – reacts directly with L-arginine in aerobic conditions, without the need for an exogenously provided keto-acid for regeneration of the PLP cofactor. To determine the product(s) of this enzyme, we first employed ESI-MS analysis to reveal that four new ions were generated: $[M+H]^+$ 146, $[M+H]^+$ 162, $[M+H]^+$ 174, and $[M+H]^+$ 190 (Figure 2). Previously, we had observed both the $[M+H]^+$ 146 and the $[M+H]^+$ 174 ions in the reaction of L-arginine with Ind4. We previously assigned the ion at $[M+H]^+$ 174 as 2-ketoarginine (**2**), and we showed that the ion at $[M+H]^+$ 146 was 4-guanidinobutyric acid (**3**), arising from the non-enzymatic decarboxylation of **2** with $H_2O_2$ produced in the course of the reaction.[17,19,20] The $[M+H]^+$ ion of 190 that we observe in this reaction could correspond to the MppP product 4-hydroxy-2-ketoarginine (**4**, configuration unknown),[14,15] which could decarboxylate in the presence of $H_2O_2$ to give 3-hydroxy-4-guanidinobutyric acid (**5**, configuration unknown), having an $[M+H]^+$ ion of $[M+H]^+$ 162.

To determine whether these ions correspond to the previously identified products, we added catalase to the reaction mixture to consume any $H_2O_2$ produced. With catalase present, we only observed the ions at $[M+H]^+$ 174 and $[M+H]^+$ 190 (Figure 2), supporting that **2** and **4** are the initial products of the enzymatic reaction that decarboxylate in the presence of $H_2O_2$ to give **3** and **5**, respectively. Furthermore, using high resolution ESI-MS to analyze all four products, we were able to confirm their elemental compositions, which correspond to the formulas for the proposed products (Table S1). To further validate the structures of these molecules, the reaction of L-arginine with the *S. cattleya* enzyme was scaled up to provide sufficient material for NMR analysis. This reaction was carried out without catalase, and the 6 h incubation time allowed complete conversion of

the initial products to the corresponding decarboxylated molecules. A combination of $^{1}$H-, $^{13}$C-, $^{1}$H-$^{1}$H COSY, $^{1}$H-$^{13}$C HSQC, and $^{1}$H-$^{13}$C HMBC NMR were employed to characterize the products. The analysis identified **3** and **5** in the reaction mixture (Figure S5), suggesting that the products of the reaction are **2** and **4**, which non-enzymatically convert to **3** and **5**, respectively, in the presence of $H_2O_2$. Despite our NMR and mass spectral analysis, the configuration of the hydroxyl in **5** (and by, extension, in **4**) remained unknown. Because this enzyme we identified catalyzes hydroxylation on an arginine-derived molecule, we named it RohP to indicate its substrate (L-arginine = R), its activity (hydroxylation = OH), and its related activity to the "P" enzymes EndP and MppP.

**Kinetics and stoichiometry of the RohP-catalyzed reaction** We hypothesized that RohP requires $O_2$ for activity the same way Ind4 and MppP do. Accordingly, we carried out the RohP reaction with L-arginine in a series of buffers and monitored the $O_2$ consumption using an oxygraph (Figure S6A). We observed an $O_2$ consumption rate of 15 μM min$^{-1}$ in 40 mM MOPS pH 7.2, a rate that decreased to 8 μM min$^{-1}$ in the presence of catalase (Figure S6B). This approximate halving of the rate of $O_2$ consumption in the presence of catalase – an enzyme that converts two molecules of $H_2O_2$ to one molecule of $O_2$ – suggests that the RohP-catalyzed reaction consumes $O_2$ with stoichiometric conversion of $O_2$ to $H_2O_2$. To further confirm the stoichiometry of the reaction, we incubated 2.5 μM RohP with 300 μM L-arginine in the presence of 0.1 mg mL$^{-1}$ Horseradish Peroxidase (Type-1) and 1 mM ABTS and quenched the reaction when 100 μM of $O_2$ was consumed. In this condition, we observed the production of 96 ± 6 μM of $H_2O_2$, indicating stoichiometric conversion of $O_2$ to $H_2O_2$. We then determined that 77 ± 4 μM of L-arginine was consumed when 100 μM of $O_2$ was consumed. This result suggests there are two reaction pathways, as we observed for Ind4. In one pathway, arginine undergoes a two-electron oxidation, with consumption of one equivalent of $O_2$. In the second pathway, arginine undergoes a four-electron oxidation, with consumption of two equivalents of $O_2$. The observed $O_2$:L-arginine stoichiometry can be rationalized if the first, less oxidizing pathway consumes twice as much L-arginine as the more oxidizing pathway. That is, for every 100 μM of $O_2$ consumed in total, 50 μM is

consumed by the first pathway to convert 50 μM of L-arginine, and 50 μM is consumed by the more oxidizing pathway to convert 25 μM of L-arginine. The first pathway leads to **2**, as observed for Ind4, whereas the second pathway should give a more oxidized product, such as **4**.

We then determined steady-state kinetic parameters for the RohP-catalyzed reaction. We determined that in the presence of air-saturated buffer, RohP has a $K_m = 40 \pm 10$ μM and a $k_{cat} = 7.8 \pm 0.6$ $min^{-1}$ for L-arginine (Figure S6C). These values are consistent with those previously reported for the related enzymes Ind4 ($K_m = 69 \pm 6$ μM, $k_{cat} = 3.5 \pm 0.1$ $min^{-1}$) and MppP ($K_m = 50 \pm 8$ μM and $k_{cat} = 13.2 \pm 0.6$ $min^{-1}$). Additionally, we determined that in the presence of saturating amounts of L-arginine, RohP has a $K_m = 78 \pm 6$ μM and a $k_{cat} = 10.2 \pm 0.2$ $min^{-1}$ for $O_2$ (Figure S6D), which can be compared to the values previously obtained for Ind4 ($K_m = 90 \pm 10$ μM, $k_{cat} = 4.6 \pm 0.1$ $min^{-1}$).

**The hydroxyl group in the RohP product derives from water, not oxygen or $H_2O_2$**

Our work demonstrates stoichiometric conversion of $O_2$ to $H_2O_2$, meaning there are no remaining oxygen atoms that could be incorporated into the product from either $O_2$ or $H_2O_2$. Thus, these stoichiometry results suggest that the hydroxyl oxygen atom in 4-hydroxy-2-ketoarginine derives from $H_2O$. To further interrogate the source of this oxygen atom, we carried out the RohP reaction in 50% $H_2{}^{18}O$ in the absence of catalase (Figure 2) and analyzed the results by LC-MS. Our results show ten unique ions. Four of these ions, those at $[M+H]^+$ 146, 162, 174, and 190, are also present in the reaction in unlabeled water, and correspond to unlabeled compounds **3**, **5**, **2**, and **4**, respectively. Additionally, four ions, those at $[M+H]^+$ 148, 164, 176, and 192, are two mass units higher, and should arise from hydrolysis of the likely imine products by $H_2{}^{18}O$, giving the corresponding labelled carbonyl oxygens. Finally, the remaining two ions, $[M+H]^+$ 166 and 194, are 4 Da heavier when compared to $[M+H]^+$ 162 and $[M+H]^+$ 190, meaning two labeled oxygens are present. One label should result from hydrolysis of the imine product by $H_2{}^{18}O$, giving a labeled carbonyl, and the second label should result from incorporation of $H_2{}^{18}O$ into the hydroxyl group. Altogether, our stoichiometric and labeling studies support that the hydroxyl oxygen derives from water, not $O_2$ or $H_2O_2$.

**UV-Visible spectrum of RohP** To further investigate the RohP-catalyzed reaction, we analyzed the UV-Visible spectra of RohP. Initially, the spectrum of RohP (30 μM) contains a single peak with a $\lambda_{max}$ at 422 nm, typical of an enzyme-PLP internal aldimine. With the addition of excess L-arginine (300 μM) we observed a decrease in the absorbance at 422 nm (Figure S7). At the same time, a peak at 515 nm, which is diagnostic of a quinonoid, increased over the 10 min incubation. Finally, a peak at 563 nm increased initially and then decreased after 5 min over the course of the experiment. Previously, we assigned a peak at 567 nm from the Ind4 reaction as a more conjugated quinonoid intermediate, and Silvaggi and coworkers assigned a similar peak at 560 nm from the MppP reaction as a more conjugated quinonoid intermediate. Our work here suggests that RohP, like Ind4 and MppP, may transition through a more conjugated quinonoid intermediate with a $\lambda_{max}$ at 563 nm.

**Crystal structure of holo-RohP** Our stoichiometric, mass spectral, and spectroscopic results suggest that RohP consumes two molecules of $O_2$ to carry out a four-electron oxidation and incorporates water to yield 4-hydroxy-2-ketoarginine. However, several questions remained unanswered. First, what is the stereochemistry of the 4-hydroxy-2-ketoarginine product? Second, what intermediates arise in such a reaction scheme? To address these questions, we turned to an X-ray crystallographic investigation of RohP.

We obtained four X-ray crystallographic structures of RohP at resolutions from 1.50 to 1.55 Å (Tables S1 and S2). Each of these structures crystallized as homodimers in space group C2. First, we determined the initial structure of holo-RohP by soaking RohP crystals with 5 mM PLP for 4 h. We used MppP (PDB: 5DJ1) as a model for molecular replacement. Holo-RohP exhibits an overall structure that is typical of other fold-type I PLP enzymes and is very similar to MppP (RMSD of 1.215 Å for Cα pairs, Figure S8A). The RohP monomer consists of a large domain (residues 25-265) and a small domain (residues 266-393) both of which exhibit an α-β-α motif. Active sites are sandwiched between the large and small domains in individual monomers and exposed to solvent. Unlike other PLP enzymes of fold-type I and similar to MppP, there are only minor contributions from one monomer to the active site of the other monomer. As was the case

for MppP, the N-terminal of the RohP holoenzyme is incomplete and missing N-terminal residues 1-25.

The RohP internal aldimine is formed between Lys235 and PLP, as was observed for Lys221 and PLP in MppP. Furthermore, all of the same residues that have stabilizing interactions with the internal aldimine in MppP are also observed in RohP (Figure S8B; Table S3). The conserved residue Lys243 (Lys229 in MppP) provides positive charge to stabilize the PLP phosphate. The position of Ser95 (Ser91 in MppP) also causes the phosphate to rotate away from the plane of the pyridine ring, as observed in MppP. Additional interactions serve to stabilize the pyridine ring of PLP. Asp198, conserved in fold-type I PLP-enzymes is located near the pyridinyl nitrogen and stabilizes positive charges on the pyridinium cation through a hydrogen bond (Figure S9A). Asn167 hydrogen bonds with the hydroxyl group of the PLP pyridine ring. As is the case with many PLP enzymes, an aromatic residue, Phe119, is located ~3.5 Å above the pyridine ring. Finally, the phosphate also forms a water-mediated hydrogen-bonding network with Asp232 (Asp218 in MppP) and Tyr92 (Tyr88 in MppP) of the other monomer of the homodimer. This structure of RohP provided a good initial model and was used to build structures produced from subsequent experiments.

**Trapping RohP the first quinonoid** The slow rate of RohP catalyzed oxidation of L-arginine afforded the opportunity to capture intermediates in the catalytic cycle by aerobic soaking of L-arginine. A RohP quinonoid intermediate structure was produced by soaking a crystal with 22 mM L-arginine for 90 s. In the resulting structure, there is no evidence of a Schiff base linkage between Lys235 and PLP. Instead, positive $F_o$-$F_c$ electron density in the shape of arginine was found to extend from the C4' aldehyde of PLP. Both the external aldimine (EA1) and quinonoid (Q1) intermediate were modelled into the electron density (Figure S10). Although both EA1 and Q1 fit well to the density, Q1 was modelled into the final structure (Figure 3A) because of its fit to the available density and our observation that a quinonoid intermediate with an absorbance at 515 nm accumulates in the reaction of RohP with L-arginine (Figure S7), suggesting that Q1 is more stable than EA1. Despite the formation of a quinonoid, the overall structure is very similar to that of holo-RohP, with the two structures superposing with an RMSD of 0.106

Å across Cα pairs. In the active site, only Asn121 exhibits a minor change in conformation, rotating towards the quinonoid (Figure S9B). Furthermore, when the quinonoid is present, the guanidium of Arg367 forms a salt bridge with the carboxylic acid of the arginine substrate. Additionally, Leu266 of the second monomer, which is unchanged in position relative to holo-RohP, now forms part of the periphery of the active site and helps to orient the guanidium end of the quinonoid. Because the N-terminal amino acids are disordered in this structure, the sidechain of the L-arginine substrate is pointed into solvent. As such, Cγ is 3.9 Å from His34 (Figure 4B), which is a residue conserved among RohP, MppP, and Ind4 (Figure S2) but not observed in other fold-type I aminotransferases.

**Trapping of a more conjugated quinonoid orders the N-terminus of RohP** When we soaked a RohP crystal with 4 mM PLP overnight and 10 mM L-arginine for 5 min, we observed the crystal change from yellow to red (Figure S11). We cryoprotected and flash-froze this red crystal. Solving the structure of this red crystal again revealed unknown positive $F_o$-$F_c$ electron density in the shape of arginine in the active site. Initially, several different intermediates were built using Phenix eLBOW and then modelled into the available $F_o$-$F_c$ density (Figures S12A-D). However, none of these intermediates gave a satisfactory fit to the available density. Thus, we employed an alternate approach, utilizing ARP/wARP[21] to build a ligand structure based upon the unknown density. The initial ARP/wARP output was adjusted in COOT, refined and found to match available omit density well (Figure S12E). This modelled ligand has bond lengths that closely match what would be expected for the more conjugated quinonoid (Q2) intermediate, containing a double bond between Cβ and Cγ positions of the arginine (Figure S12F). To interrogate whether modeling Q2 was reasonable for such a red crystal, we carried out spectroscopic analysis on other frozen red crystals using the microspectrophotometer outfitted on beamline 9-2 at the Stanford Synchrotron Radiation Lightsource. This work revealed that such red crystals have peaks with a $\lambda_{max}$ of 515 and 563 nm (Figure S13A), matching the peaks observed by UV-Visible spectroscopy in solution (Figure S7). We solved the structure of one of these crystals, which diffracts to lower, 2.0 Å resolution, revealing that it too contains a PLP adduct (Figures S13B, C). As we observe a more

conjugated quinonoid intermediate in the UV-visible spectra both in solution and in crystallo (Figures S7 and S13A), it is likely that Q2 is a more stable intermediate than a more conjugated external aldimine (EA2). Therefore, we built Q2 into the final structure based on the ARP/wARP coordinates (Figures 3B and S12E). However, the ~1.5 Å resolution of this structure does not allow us to unambiguously assign the pattern of double bonds. Furthermore, a mixture of intermediates may contribute to the density we observed.

In this structure of the Q2 intermediate, electron density for residues 13-25 of the N-terminus is present, forming a small α-helix that closes off the active site, isolating the active site from bulk solvent (Figure 3B**)**. With the ordering of the N-terminus, the amide nitrogen of Leu16 forms a hydrogen bond with Asp120. Additionally, the hydroxyl sidechain of Thr17 forms a hydrogen bond with the guanidium group of Q2 and pushes the guanidium deeper into the active site where it forms additional hydrogen bonds with Ser95 and the carbonyl oxygen of Val264. The conserved residue Glu20 becomes ordered near the carboxylic acid and Cβ of Q2. Phe119 also exhibits a dual conformation, with the additional conformer rotating from its previous position above the pyridine ring to a position ~3.5 Å above the carboxylic acid of Q2. Asn121 also moves ~180° from its previous position to partially occupy the area that was vacated by the rotation of Phe119. Collectively, these changes push Q2 deeper into the active site, into a position where Glu20 is 4.0 Å away from Cβ and His34 is 3.2 Å and 3.5 Å away from Cβ and Cδ, respectively, of the arginine substrate (Figure 4C).

**Structure of RohP-product complex** We obtained a final snapshot of the RohP catalytic cycle by soaking RohP crystals with 10 mM L-arginine overnight. During this experiment, the crystal changed from yellow to red and then back to yellow. We cryoprotected and flash-froze the resulting yellow crystal. The structure we obtained has N-terminal residues 14-25 present, though the density of these residues in chain B is weaker. Therefore, these residues were modelled with an occupancy of ~0.7-0.8 in chain B, compared to full occupancy in chain A. The active site of the enzyme also remains largely unchanged compared to the Q2 structure, with Asn121 remaining flipped relative to its initial position, and Phe119 exhibiting a dual conformation away from the pyridine

ring of PLP. However, in this structure, PLP has again formed an internal aldimine with Lys235 (Figure S9D). Strong $F_o$-$F_c$ density was present above the internal aldimine, displaying a shape consistent with a product containing a 4-hydroxy group. Both the enamine and hydrolysis product of the imine tautomer were modelled into the available density to determine their fit (Figure S14); the larger negative density over the enamine double bond led us to model 4-hydroxy-2-ketoarginine into the final structure. We suspect that the dynamic nature of the *N*-terminus should allow for hydrolysis of the enamine product over the extended incubation period. As the stereochemistry of the 4-hydroxyl was still undetermined, both the *R* and *S* enantiomers of the molecule were modelled into the positive $F_o$-$F_c$ density present in the active site (Figure 5). Refinement of the *R*-enantiomer produced strong negative $F_o$-$F_c$ density around the hydroxyl group, while the same refinement of the *S*-enantiomer produced no negative $F_o$-$F_c$ density around the hydroxyl group. Identical results were also observed for both enantiomers of the enamine product (Figure S14). These results support that RohP catalyzes the production of (*S*)-4-hydroxy-2-ketoarginine (**4**) from L-arginine.

**Characterization of the RohP-His34Ala variant** Based upon our crystallographic results, His34 appears likely to be involved in the installation of the 4-hydroxyl group, due to its position relative to the quinonoid intermediates (Figure 4). To probe the function of His34 we created a His34Ala variant of RohP with site-directed mutagenesis. ESI-MS analysis was again employed to determine the product(s) of the His34Ala variant. The production of **4** was abolished, however, the variant was still able to produce **2**. The corresponding decarboxylation product **3** was also detected (Figure S15). That this variant was only able to perform one oxidation, and no other intermediates were detected, suggests that His34 may also be involved in catalyzing the second oxidation of the arginine substrate and possibly the final hydration reaction.

## Discussion

In this work, we investigate RohP, an enzyme that uses pyridoxal phosphate to catalyze the transformation of L-arginine and $O_2$ to two products: 2-ketoarginine (**2**) and (*S*)-4-hydroxy-2-ketoarginine (**4**). While previous studies by Eguchi and Silvaggi highlighted

this enzymatic reaction, the key question of how an enzyme uses PLP and $O_2$ to hydroxylate an unactivated, $sp^3$-hybridized carbon remained unaddressed. Here, we use detailed mass spectral, kinetic, stoichiometric, and X-ray crystallographic analysis to build a firm mechanistic framework for understanding this group of PLP-, $O_2$-dependent hydroxylases. Our work demonstrates that RohP and the oxidase Ind4 share many key features: both stoichiometrically convert $O_2$ to $H_2O_2$, both generate quinonoid and conjugated quinonoid intermediates, and both produce the less oxidized product, 2-ketoarginine, which results from hydrolysis of the corresponding imine. The enzymes differ only in whether they produce didehydroarginine or (*S*)-4-hydroxy-2-ketoarginine. From our X-ray crystal structures containing trapped quinonoid and conjugated quinonoid intermediates, along with a structure with product bound, we unveil a shared mechanism whereby both enzymes can catalyze a four-electron oxidation of L-arginine. However, only RohP can utilize water to carry out a stereospecific alkene hydration.

Our crystallographic work shows that RohP forms an external aldimine at the α-amino group of arginine, exactly as would be expected for a PLP-dependent aminotransferase. In our mechanistic proposal (Figure 6), we suggest that the Cα proton of the external aldimine (EA1) is abstracted by Lys235, with the resulting anionic species stabilized by formation of a quinonoid intermediate (Q1). Q1 is a typical intermediate in PLP-dependent aminotransferases, one that we also observe accumulate by UV-Visible spectroscopy. We then propose that Q1, as for Ind4, reacts directly with $O_2$, oxidizing the bound amino acid and releasing $H_2O_2$. The exact mechanism of how $O_2$ interacts with Q1 is currently unknown, as is the mechanism for release of $H_2O_2$. After oxidation, the resulting external aldimine intermediate (EA2) forms. This intermediate can undergo one of two fates: it can either be attacked by Lys235, which will reform the internal aldimine and release an enamine product, which tautomerizes to the imine and is then hydrolyzed to give **2**. Alternatively, the oxidized intermediate can remain in the active site. If it remains in the active site, the Cγ proton can undergo rapid deprotonation by the adjacent His34, shuttling electron density into the cofactor to give the more conjugated quinonoid (Q2) intermediate. Then, a second molecule of $O_2$ could react with Q2, again oxidize the substrate, and release a second molecule of $H_2O_2$. Now, the PLP-tethered didehydroarginine could undergo hydration. One possible scenario is that the double

bond between Cγ-Cδ is first protonated at the Cδ position. The resulting carbocation at Cγ could be stabilized through resonance with density from the PLP pyridine ring. Now His34 deprotonates an adjacent water to insert the hydroxyl group at Cγ and give the resulting PLP-tethered final product. The stereospecificity of the hydration appears to be promoted by the positioning of His34, which is positioned to the *si* face of the alkene. At the same time, the phosphate of PLP occludes solvent access to the *re* face of the alkene. To complete the catalytic cycle, the 4-hydroxy product is then released when Lys235 attacks to release the enamine with the concomitant formation of the RohP-PLP internal aldimine. The imine tautomer is then hydrolyzed by water to produce the final product **4**.

Our work raises exciting questions about $O_2$, PLP-dependent oxidases. First, what are the structural features that distinguish arginine oxidases like Ind4 from arginine hydroxylases like RohP and MppP? We suggest that the remarkable feat of RohP – installation of a hydroxyl group – could be the stereospecific hydration of a PLP-tethered didehydroarginine. If this possibility is true, what causes the hydroxylase RohP to catalyze the hydration, whereas the oxidase Ind4 releases didehydroarginine as a product? The two types of enzymes have all residues conserved in their active sites – including His34 – suggesting that other residues will be key to determining the product outcome (Table S3). An Ind4 structure will be essential for pinpointing which residues are critical to determining product outcome. Second, in both RohP-like and Ind4-like enzymes, **2** is produced. Is the production of **2** an unavoidable waste product for such L-arginine, PLP-, $O_2$-dependent enzymes, or is there a purpose for production of **2**? Elucidation of the full biosynthetic pathway will begin to address this issue. Finally, an unresolved question is why a select group of PLP-dependent enzymes are able to use $O_2$ to catalyze oxidation reactions and how $O_2$ is activated during catalysis.[8,11,12] Answers to these questions await further study.

## METHODS

***General methods*** Primers were purchased from Integrated DNA Technologies. DNA sequencing was carried out by NAPS Unit DNA Sequencing Facility (The University of British Columbia). Reagents were purchased from Anatrace, Bio Basic Inc., Gold

Biotechnology, Hampton Research, New England Biolabs (NEB), Thermo Fisher Scientific Canada, and VWR International.

***Cloning, expression, and purification*** The gene *rohP*, which encoded RohP as originally annotated, was amplified from genomic DNA of *S. cattleya* (NRRL 8057, DSM 46488) by the polymerase chain reaction using the primers RohP-F 5′-AGCAGCCATATGAAGTACAACCTCGCCGACGCC-3′ (NdeI site underlined) and RohP-R 5′-AGTAGTCTCGAGTCAGCGGCCATGGCGGTC-3′ (XhoI site underlined). The re-annotated *rohP*, which coded for the active form of RohP with an intact N-terminus, was similarly amplified using the primers RohP-F-2 5′-AGCAGCCATATGCACCCGCAAG-CGACC-3′ and RohP-R. The products were digested with NdeI and XhoI, and ligated into similarly digested plasmid pET28a (EMD Millipore) to produce a N-terminal $His_6$-tagged protein. Site-directed mutagenesis of RohP was performed using the Q5 Site-Directed Mutagenesis Kit (New England Biolabs), using the primers H34A-F 5′-CGCCGACGCCGCCACCCACCAG-3′ and H34A-R 5′-GAGGTTGTACTTCATGGTCA-GCGCCTGGATCTCGTG-3′. The nucleotide sequence of the cloned *rohP* was confirmed, and the plasmid was transformed into *E. coli* BL21 (DE3) cells for protein production.

*E. coli* cell cultures were grown at 37 °C in Luria-Bertani (LB) medium containing 50 μg/mL kanamycin to an $OD_{600}$ of 0.8–1.0, and then cooled to 16 °C. Protein expression was induced with 0.1 mM β-D-1-thiogalactopyranoside (IPTG), and the cultures were grown for an additional 16 h at 16 °C. Cells were harvested by centrifugation and frozen at –20 °C until protein purification.

For purification, the cells were thawed and re-suspended in 20 mM HEPES, 50 mM NaCl (pH 7.5) buffer and sonicated to lyse the cells. The lysate was then centrifuged at 40,500 *g* for 45 min to remove insoluble material. The lysate was then applied to a column containing ~1 mL Chelating Sepharose™ Fast Flow resin (GE Lifesciences) charged with $NiSO_4 \cdot 6H_2O$. The lysate was gravity filtered through the resin, and the resin was washed with 20 mL of 20 mM HEPES, 50 mM NaCl (pH 7.5) buffer. The column was then washed with 5 mL portions of 20 mM HEPES, 50 mM NaCl (pH 7.5) containing 5, 10, 20, 50, 100, 200, 300, and 500 mM imidazole in a stepwise manner to elute the protein. The fractions containing RohP could be identified by the yellow color,

and most of the protein eluted in the fractions that contained 200 and 300 mM imidazole. The RohP containing fractions were combined and concentrated to a volume of ~5 mL using an Amicon Ultra Centrifugal filter (10,000 molecular weight cut-off, EMD-Millipore). The concentrated fraction was loaded into a HiLoad™ Superdex 16/600 Superdex column (GE Amersham Biosciences) pre-equilibrated with 20 mM HEPES, 50 mM NaCl (pH 7.5) buffer. The protein was eluted using a flow rate of 1 mL $min^{-1}$. The fractions containing purified RohP were pooled to a final concentration of ~50 μM and dialyzed against HEPES buffer containing 250 μM PLP for 16 h. Excess PLP was removed by further dialysis with 20 mM HEPES, 50 mM NaCl (pH 7.5). Finally, RohP was concentrated to ~20 mg $mL^{-1}$ by centrifugation with an ultra centrifugal filter (10,000 molecular weight cut-off, EMD-Millipore). At this concentration, the purified RohP remained stable at 4 °C and was stored in the dark.

***In vitro biochemical assays and product analysis*** Initial *in vitro* reactions (100 μL) contained 30 μM RohP and 1 mM L-arginine, in 20 mM Tris, 50 mM NaCl (pH 7.5) buffer and proceeded for 16 h at room temperature. HPLC analysis of the reaction was carried out after pre-column derivatization with dansyl-chloride (DNS-Cl). A reaction mixture of 50 μL was treated with 80 mM $Li_2CO_3$, 70 μL of $CH_3CN$, and 30 μL of 5 mM DNS-Cl dissolved in $CH_3CN$. The reaction was carried out at room temperature for 1 h and then 40 μL of 2% ethylamine was added to the mixture to react with excess DNS-Cl. The mixture was centrifuged, and 20 μL of the supernatant was subjected to HPLC analysis. HPLC analysis was carried out on a 1260 HPLC apparatus (Agilent), using a Luna C18(2), 5 μm, 4.6 mm ID × 250 mm column (Phenomenex). Elution was performed at 0.5 mL $min^{-1}$ using a mobile-phase consisting of a linear gradient of water and acetonitrile ((v/v): 95:5 to 50:50, 0 to 15 min; 0:100, 15 to 22 min), with both solvents containing 0.05% (v/v) trifluoroacetic acid. DNS-Arg was detected at a wavelength of 330 nm.

*In vitro* assays for ESI-MS analysis contained 10 μM RohP and 1 mM L-arginine, in 20 mM HEPES, 50 mM NaCl (pH 7.5) buffer in a 100 μL reaction mixture. These reactions were carried out for 4 h at room temperature and then quenched with an equal volume of methanol. Precipitated protein was removed by centrifugation and 10 μL of

the supernatant was subjected to ESI-MS analysis. MS analysis was performed with a 6120 Quadrupole LC/MS system (Agilent) operated in positive ion mode.

***NMR analysis of RohP reaction products*** The reaction mixture (5 mL) contained 20 μM RohP, and 10 mM L-arginine in 20 mM sodium phosphate buffer (pH 7.2). The mixture was incubated in an unsealed 50 mL vial at 25 °C and shaken at 120 rpm for 6 h. The solvent was then evaporated overnight using a SpeedVac plus vacuum concentrator. The dried solids were re-suspended in 600 μL $D_2O$ and centrifuged to remove any residual undissolved solids prior to NMR analysis. All spectra were acquired utilizing a Bruker Avance 600 MHz spectrophotometer.

***Steady-state kinetics for the RohP reaction*** Kinetic assays were performed by monitoring the consumption of $O_2$ using a Clark-type polarographic $O_2$ electrode (Hansatech, Pentney, UK) similar to the method described previously.[17] The electrode was calibrated daily using air-saturated water and sodium hydrosulfite according to the manufacturer's instructions. The standard assay was performed in 1 mL of air-saturated 40 mM MOPS ($I$ = 0.1 M, pH 7.2) at 25 °C containing 500 μM L-arginine. The reaction was initiated with the addition of RohP to 1 μM. The observed rates were corrected with background $O_2$ consumption prior to reaction initiation. The effect of pH on the rate of the RohP-catalyzed reaction was evaluated using air-saturated 20 mM buffers ($I$ = 0.1 M) of MES (pH 6.0), PIPES (pH 6.7), MOPS (pH 7.2), HEPES (pH 7.4), HEPPS (pH 8.0), and TAPS (pH 8.5).

The steady-state kinetic parameters of RohP with respect to L-arginine were determined at ambient oxygen levels by varying the concentration of L-arginine (8 – 500 μM) using 1 μM and 5 μM of RohP, respectively. The steady-state kinetic parameters of RohP with respect to oxygen were measured using 17 – 685 μM $O_2$ at an L-arginine concentration of 500 mM. $O_2$ concentrations were established by bubbling mixtures of $O_2$ and $N_2$ into the reaction chamber prior to reaction initiation. The final oxygen concentrations were standardized to the level of air-saturated buffer before the gas bubbling. Kinetic parameters were determined either by least-squares fitting of the Michaelis-Menten equation to the data using LEONORA or by Hill equation using Origin 8.1 (OriginLab corp., Northampton, MA).

***Stoichiometry of the RohP reaction*** The production of $H_2O_2$ was evaluated by comparing the reaction rates catalyzed by 2.5 μM RohP and 0.3 mM L-arginine in the presence or absence of ~4000 U of catalase. $H_2O_2$ production was also measured colorimetrically by supplementing the reaction with 0.1 mg $mL^{-1}$ horseradish peroxidase (HRP) (Type-1) and 1 mM 2,2'-azino-bis(3-ethylbenzothiazoline-6-sulphonic acid) (ABTS). Upon the consumption of 100 μM oxygen, the reaction was quenched with 1 volume of 10% TCA. The experimental values were compared to a calibration curve of $H_2O_2$.

For quantification of the L-arginine:$O_2$ stoichiometry, reaction mixtures (1 mL) containing 12 μM RohP and 250 μM L-arginine in 40 mM MOPS ($I$ = 0.1 M, pH 7.2) buffer were incubated at 25 °C. The mixture was equilibrated to ambient $O_2$ levels prior to the addition of RohP. Upon addition of RohP the $O_2$ concentration was monitored by Oxygraph and the reaction was quenched with one volume of MeOH after 100 μM of $O_2$ was consumed. The L-arginine remaining after the reaction with RohP by was quantified by HPLC after pre-column derivatization with *o*-phthaldialdehyde (OPA)/mercaptopropionic acid (MPA). The quenched solution was incubated with 1 volume of 0.4 M borate buffer (pH 10.2) and 1 volume of OPA/MPA solution (1 mg $mL^{-1}$ OPA, 0.1% (v/v) MPA in 0.1 M borate buffer (pH 10.2)) for 3 min before HPLC analysis. HPLC analysis was carried out on a 1260 HPLC apparatus (Agilent), using a Poroshell 120, EC-C18, 2.7 μm, 4.6 mm ID × 50 mm column (Agilent). Elution was performed at 1.0 mL $min^{-1}$ using a mobile-phase consisting of a linear-gradient of water and acetonitrile ((v/v): 98:2, 0 to 1 min; 80:20, 1 to 5 min; 50:50, 5 to 6.5 min; 0:100, 6.5 to 8 min; 98:2, 8 to 10 min), with both solvents containing 0.05% (v/v) trifluoroacetic acid. Derivatized L-arginine was detected at a wavelength of 330 nm. The experimental values were compared to a calibration curve of L-arginine that was done using the same conditions. The data are reported as mean values ± s.d., with n = 5.

***Spectroscopic analysis of the RohP reaction*** Aerobic reaction mixtures (1 mL) were prepared in a quartz cuvette with a path length of 1 cm and contained 30 μM of enzyme and 300 μM of substrate in 20 mM HEPES, 50 mM NaCl, pH 7.5. All solutions were room temperature and air saturated with oxygen. The reaction was initiated upon addition of substrate. Spectra were recorded using a Varian Cary 100 Bio UV-Vis spectrophotometer (Agilent).

***Crystallization*** Initial crystallization conditions were identified by screening 4 mg $mL^{-1}$ RohP against the Index HT Screen (Hampton Research) and Top96 Crystal Screen (Anatrace). Optimization of the initial crystallization conditions was carried out at room temperature using hanging drop vapor diffusion. Diffraction-quality crystals were obtained by mixing 1.5 μL of 8 mg $mL^{-1}$ protein and an equal volume of a crystallization solution composed of 0.2 M sodium malonate (pH 7.0), and 16–20% (w/v) PEG 3350, using hanging drop vapor diffusion over a 500 μL reservoir of the crystallization solution. Large, yellow crystals appeared after approximately 7 d, though some crystals took up to 4 weeks to form under these conditions.

The structures of RohP in complex with intermediates and product were obtained by adding solutions of PLP to the ~3 μL drops containing crystals of RohP, soaking overnight, and then adding L-arginine solutions for timed soaks. The structure of the holo-RohP resulted from adding 1 μL of 20 mM PLP to a drop containing crystals for an overnight soak, giving a final concentration of 5 mM PLP. The structure of the first RohP quinonoid intermediate (Q1) resulted from adding 0.5 μL 20 mM PLP for an overnight soak and then adding 1 μL 100 mM L-arginine for 90 s, giving final concentrations of 2.2 mM PLP and 22 mM L-arginine. The structure of the second RohP quinonoid intermediate (Q2) resulted from adding 1.0 μL 20 mM PLP for an overnight soak and then adding 1 μL 50 mM L-arginine for 5 min, giving final concentrations of 4 mM PLP and 10 mM L-arginine. The RohP-4-hydroxy-2-ketoarginine structure resulted from adding 1.0 μL 20 mM PLP and 1 μL 50 mM L-arginine for an overnight soak, giving final concentrations of 4 mM PLP and 10 mM L-arginine. After soaking as described, the crystals were cryoprotected using solution composed of 0.2 M sodium malonate (pH 7.0), 15% (w/v) PEG 3350, and 20% (v/v) ethylene glycol and flash-frozen in liquid nitrogen prior to X-ray data collection.

***Data collection, structure determination and model refinement*** X-ray diffraction data were collected at the Canadian Light Source (Saskatoon, Canada), beamline 08ID-1, at a wavelength of 0.97949 Å using MX300-HE and Pilatus 6M detectors. UV-Visible spectroscopic data of RohP crystals were collected using the microspectrophotometer at beamline BL9-2 at the Stanford Synchrotron Radiation Light Source (Menlo Park, United States). All data sets were integrated using iMOSFLM,[22] and scaled using AIMLESS.[23]

RohP crystallized with two units in the asymmetric unit, forming a homodimer in the space group $C_2$. The crystal structures of each RohP complex was phased by PHASER-MR[24] in the Phenix software package, using the L-arginine, γ-hydroxylase SwMppP as a model (PDB: 5DJ1 chain D, 32% identity across 393 amino acid residues). The initial results from molecular replacement were input into Phenix Autobuild[25] for additional model building. The Autobuild output was subjected to several rounds of manual inspection and building in COOT,[26] and refinement in phenix.refine[27] using translation-liberation-screw (TLS) refinement. Alternate conformations of side chains and molecules from the crystallization solution were added to the model where appropriate. Solvent molecules were added automatically in phenix.refine and examined manually in COOT. Refinement statistics are listed in Table 1. Non-standard ligand restraints were generated using Phenix eLBOW.[28] The second quinonoid intermediate (Q2) was initially fit to the $F_o$-$F_c$ omit density using ARP/wARP version 7.6.[21] The coordinates generated were used to produce a restraint file containing the ARP/wARP optimized geometry, and the entire structure was subjected to additional refinement in phenix.refine.

The holo-RohP structure has the *N*-terminus through residue 26 disordered in both chains. The first RohP quinonoid intermediate (Q1) structure has the *N*-terminus through residue 25 disordered in both chains. The second RohP quinonoid intermediate (Q2) structure has the *N*-terminus through residue 13 disordered in both chains. The structure of the RohP with (*S*)-4-hydroxy-2-ketoarginine in the active site has the *N*-terminus through residue 13 disordered in Chain A and through residue 14 disordered in Chain B. In all structures, *C*-terminal residues 391–393 are disordered in each monomer, except in Chain B of both quinonoid structures, where residues 392–393 are disordered.

## ASSOCIATED CONTENT

### Supporting Information

Supporting Information is available free of charge on the ACS Publications website at DOI:

High resolution ESI-MS data, X-ray collection data, Supporting Figures S1-S15

### Data Deposition

The atomic coordinates and structure factors for the crystal structures reported have been deposited in the Protein Data Bank. PDB ID Codes 6C3A (RohP-4-hydroxy-2-ketoarginine), 6C3B (RohP-holoenzyme), 6C3C (RohP-quinonoid I) and 6C3D (RohP-quinonoid II).

**Author Information**

**Corresponding Author**

*ksryan@chem.ubc.ca

**ORCID**

Jason B. Hedges: 0000-0003-2922-0085

Eugene Kuatsjah: 0000-0002-8793-2331

Yi-Ling Du: 0000-0001-7072-4803

Lindsay D. Eltis: 0000-0002-6774-8158

Katherine S. Ryan: 0000-0003-1643-1940

**Declaration of Interests** The authors declare no competing interests.

**Acknowledgements** We thank M. Higgins for assistance with the initial X-ray crystallographic work. Our work was supported by funding from the Natural Sciences and Engineering Research Council of Canada (RGPIN-2016-03778 to K.S.R., and 171359-13 to L.D.E.), the Alfred P. Sloan Foundation (FG-20166503 to K.S.R.), and the Canadian Institutes of Health Research (FDN-148381 and 201312MSH-322191-209186 to K.S.R.). L.D.E. holds a Tier 1 Canada Research Chair. Research described in this paper was performed using beamline 08ID-1 at the Canadian Light Source and beamline 9-2 at the Stanford Synchrotron Radiation Light Source.

**References**

(1) Labinger, J. A., and Bercaw, J. E. (2002) Understanding and exploiting C-H bond activation. *Nature 417*, 507–514.

(2) Roudesly, F., Oble, J., and Poli, G. (2017) Metal-catalyzed C-H activation/functionalization: The fundamentals. *J. Mol. Catal. Chem. 426*, 275–296.

(3) Helmetag, V., Samel, S. A., Thomas, M. G., Marahiel, M. A., and Essen, L.-O. (2009) Structural basis for the erythro-stereospecificity of the L-arginine oxygenase VioC in viomycin biosynthesis. *FEBS J. 276*, 3669–3682.
(4) Ge, W., Wolf, A., Feng, T., Ho, C., Sekirnik, R., Zayer, A., Granatino, N., Cockman, M. E., Loenarz, C., Loik, N. D., Hardy, A. P., Claridge, T. D. W., Hamed, R. B., Chowdhury, R., Gong, L., Robinson, C. V., Trudgian, D. C., Jiang, M., Mackeen, M. M., McCullagh, J. S., Gordiyenko, Y., Thalhammer, A., Yamamoto, A., Yang, M., Liu-Yi, P., Zhang, Z., Schmidt-Zachmann, M., Kessler, B. M., Ratcliffe, P. J., Preston, G. M., Coleman, M. L., and Schofield, C. J. (2012) Oxygenase-catalyzed ribosome hydroxylation occurs in prokaryotes and humans. *Nat. Chem. Biol. 8*, 960–962.
(5) Chang, C.-Y., Lyu, S.-Y., Liu, Y.-C., Hsu, N.-S., Wu, C.-C., Tang, C.-F., Lin, K.-H., Ho, J.-Y., Wu, C.-J., Tsai, M.-D., and Li, T.-L. (2014) Biosynthesis of streptolidine involved two unexpected intermediates produced by a dihydroxylase and a cyclase through unusual mechanisms. *Angew. Chem. Int. Ed. Engl. 53*, 1943–1948.
(6) Phillips, R. S. (2015) Chemistry and diversity of pyridoxal-5′-phosphate dependent enzymes. *Biochim. Biophys. Acta BBA - Proteins Proteomics 1854*, 1167–1174.
(7) Toney, M. D. (2011) Controlling reaction specificity in pyridoxal phosphate enzymes. *Biochim. Biophys. Acta BBA - Proteins Proteomics 1814*, 1407–1418.
(8) Bunik, V. I., Schloss, J. V., Pinto, J. T., Dudareva, N., and Cooper, A. J. L. (2011) A survey of oxidative paracatalytic reactions catalyzed by enzymes that generate carbanionic intermediates: implications for ROS production, cancer etiology, and neurodegenerative diseases. *Adv. Enzymol. Relat. Areas Mol. Biol. 77*, 307–360.
(9) Bertoldi, M., Cellini, B., Montioli, R., and Borri Voltattorni, C. (2008) Insights into the mechanism of oxidative deamination catalyzed by DOPA decarboxylase. *Biochemistry 47*, 7187–7195.
(10) Sakai, K., Miyasako, Y., Nagatomo, H., Watanabe, H., Wakayama, M., and Moriguchi, M. (1997) L-Ornithine decarboxylase from *Hafnia alvei* has a novel L-ornithine oxidase activity. *J. Biochem. 122*, 961–968.
(11) Kaminaga, Y., Schnepp, J., Peel, G., Kish, C. M., Ben-Nissan, G., Weiss, D., Orlova, I., Lavie, O., Rhodes, D., Wood, K., Porterfield, D. M., Cooper, A. J. L., Schloss, J. V., Pichersky, E., Vainstein, A., and Dudareva, N. (2006) Plant phenylacetaldehyde synthase is a bifunctional homotetrameric enzyme that catalyzes phenylalanine decarboxylation and oxidation. *J. Biol. Chem. 281*, 23357–23366.
(12) Wang, M., Zhao, Q., Zhang, Q., and Liu, W. (2016) Differences in PLP-dependent cysteinyl processing lead to diverse *S*-functionalization of lincosamide antibiotics. *J. Am. Chem. Soc. 138*, 6348–6351.
(13) Huang, Y., Liu, X., Cui, Z., Wiegmann, D., Niro, G., Ducho, C., Song, Y., Yang, Z., and Van Lanen, S. G. (2018) Pyridoxal-5′-phosphate as an oxygenase cofactor: discovery of a carboxamide-forming, α-amino acid monooxygenase-decarboxylase. *Proc. Natl. Acad. Sci. U. S. A. 115*, 974–979.
(14) Nakane, A., Nakamura, T., and Eguchi, Y. (1977) A novel metabolic fate of arginine in *Streptomyces eurocidicus*. Partial resolution of the pathway and identification of an intermediate. *J. Biol. Chem. 252*, 5267–5273.
(15) Han, L., Schwabacher, A. W., Moran, G. R., and Silvaggi, N. R. (2015) *Streptomyces wadayamensis* MppP is a pyridoxal 5′-phosphate-dependent L-arginine α-

deaminase, γ-hydroxylase in the enduracididine biosynthetic pathway. *Biochemistry 54*, 7029–7040.
(16) Du, Y.-L., Alkhalaf, L. M., and Ryan, K. S. (2015) In vitro reconstitution of indolmycin biosynthesis reveals the molecular basis of oxazolinone assembly. *Proc. Natl. Acad. Sci. U. S. A. 112*, 2717–2722.
(17) Du, Y.-L., Singh, R., Alkhalaf, L. M., Kuatsjah, E., He, H.-Y., Eltis, L. D., and Ryan, K. S. (2016) A pyridoxal phosphate-dependent enzyme that oxidizes an unactivated carbon-carbon bond. *Nat. Chem. Biol. 12*, 194–199.
(18) Yin, X., and Zabriskie, T. M. (2006) The enduracidin biosynthetic gene cluster from *Streptomyces fungicidicus*. *Microbiol. 152*, 2969–2983.
(19) Li, C., and Lu, C.-D. (2009) Arginine racemization by coupled catabolic and anabolic dehydrogenases. *Proc. Natl. Acad. Sci. U. S. A. 106*, 906–911.
(20) Vlessis, A. A., Bartos, D., and Trunkey, D. (1990) Importance of spontaneous alpha-ketoacid decarboxylation in experiments involving peroxide. *Biochem. Biophys. Res. Commun. 170*, 1281–1287.
(21) Langer, G., Cohen, S. X., Lamzin, V. S., and Perrakis, A. (2008) Automated macromolecular model building for X-ray crystallography using ARP/wARP version 7. *Nat. Protoc. 3*, 1171–1179.
(22) Battye, T. G. G., Kontogiannis, L., Johnson, O., Powell, H. R., and Leslie, A. G. W. (2011) *iMOSFLM* : a new graphical interface for diffraction-image processing with *MOSFLM*. *Acta Crystallogr. D Biol. Crystallogr. 67*, 271–281.
(23) Evans, P. R., and Murshudov, G. N. (2013) How good are my data and what is the resolution? *Acta Crystallogr. D Biol. Crystallogr. 69*, 1204–1214.
(24) McCoy, A. J., Grosse-Kunstleve, R. W., Adams, P. D., Winn, M. D., Storoni, L. C., and Read, R. J. (2007) *Phaser* crystallographic software. *J. Appl. Crystallogr. 40*, 658–674.
(25) Terwilliger, T. C., Grosse-Kunstleve, R. W., Afonine, P. V., Moriarty, N. W., Zwart, P. H., Hung, L.-W., Read, R. J., and Adams, P. D. (2008) Iterative model building, structure refinement and density modification with the *PHENIX AutoBuild* wizard. *Acta Crystallogr. D Biol. Crystallogr. 64*, 61–69.
(26) Emsley, P., and Cowtan, K. (2004) *Coot* : model-building tools for molecular graphics. *Acta Crystallogr. D Biol. Crystallogr. 60*, 2126–2132.
(27) Afonine, P. V., Mustyakimov, M., Grosse-Kunstleve, R. W., Moriarty, N. W., Langan, P., and Adams, P. D. (2010) Joint X-ray and neutron refinement with *phenix.refine*. *Acta Crystallogr. D Biol. Crystallogr. 66*, 1153–1163.
(28) Moriarty, N. W., Grosse-Kunstleve, R. W., and Adams, P. D. (2009) *electronic Ligand Builder and Optimization Workbench* (*eLBOW*): a tool for ligand coordinate and restraint generation. *Acta Crystallogr. D Biol. Crystallogr. 65*, 1074–1080.

**Figure Legends:**

**Figure 1.** Ind4- and RohP-catalyzed reactions. $[M+H]^+$ ions observed from both RohP and Ind4-catalyzed reactions are shown in purple, from only the RohP-catalyzed reactions are in red, and from only the Ind4-catalyzed reaction are in blue. Molecules in gray arise from non-enzymatic reactions with $H_2O_2$.

**Figure 2.** RohP-catalyzed oxidation of L-arginine. Liquid chromatography-mass spectrometry analysis of the products of the RohP reaction with L-arginine (L-Arg). The reaction conditions are indicated above each spectrum, and representative integrated total ion chromatograms for each reaction are shown.

**Figure 3.** Modelling of RohP-quinonoid intermediates. Left Panel: (a) The first quinonoid intermediate (Q1) modelled into the density present in the active site of the first RohP intermediate structure. (b) The second quinonoid intermediate (Q2) with a double bond between arginine Cβ and Cγ modelled into the density present in the active site of the second intermediate structure. Both $F_o$-$F_c$ omit maps are displayed in green and contoured at 3.0 σ. Middle panel: Depicts the entire protein structure as modelled in each structure. The two monomers are indicated with light and dark coloring. The *N*-terminal helix, absent in holo-RohP, is colored magenta here. Right panel: View of active sites, with nearby conserved residues surrounding the quinonoid intermediates depicted as sticks.

**Figure 4.** Distances between modelled quinonoid intermediates and conserved residues Glu20 and His34 in Chain A of the RohP homodimer. (a) The RohP holoenzyme has only a water molecule (red sphere) positioned 2.4 Å from His34. (b) The N-terminus and Glu20 are absent in the RohP-quinonoid I. His34 is positioned 3.9 Å from the Cγ atom of the bound substrate and 2.5 Å from a water molecule. (c) In the RohP-quinonoid II, the N-terminus is ordered, including Glu20, which is now positioned 4.0 Å from the Cβ of the bound substrate. Furthermore, the new positioning of the amino acid substrate places its Cβ and Cδ atoms 3.2 Å and 3.5 Å, respectively, from His34. No ordered water was

present near His34. (d) The product (*S*)-4-hydroxy-2-ketoarginine has its Cβ 3.3 Å from Glu20 and its Cδ 3.6 Å from His34. The 4' hydroxyl group is positioned 2.7 Å from His34.

**Figure 5.** Possible stereoisomers of 4-hydroxy-2-ketoarginine. (a) The *R*-enantiomer modelled into $F_o$-$F_c$ omit density present in the active site. (b) The density present around the *R*-enantiomer after refinement using Refmac. (c) The *S*-enantiomer modelled into $F_o$-$F_c$ omit density present in the active site. (d) The density present around the *S*-enantiomer after refinement using Refmac. The $F_o$-$F_c$ maps are contoured at 3.0 σ with positive and negative density indicated as green and red, respectively. The $2F_o$-$F_c$ maps are contoured at 1.0 σ in gray. Ligands were built using eLBOW in the Phenix software suite.

**Figure 6.** Proposed mechanism of the RohP catalyzed reaction to give **4**.

**Table 1.** RohP X-Ray Refinement Statistics

| | Holo-RohP [**6C3B**] | Quinonoid I (Q1) [**6C3C**] | Quinonoid II (Q2) [**6C3D**] | Int. Aldimine – Product [**6C3A**] |
|---|---|---|---|---|
| **Refinement** | | | | |
| $R_{work}$[a] | 0.1522 (0.2332) | 0.1624 (0.2409) | 0.1599 (0.2326) | 0.1528 (0.2251) |
| $R_{free}$[a] | 0.1725 (0.2476) | 0.1866 (0.2601) | 0.1856 (0.2454) | 0.1729 (0.2505) |
| No. non-hydrogen atoms | 6859 | 7079 | 7079 | 7121 |
| Protein | 5951 | 5942 | 6123 | 6140 |
| Solvent | 828 | 1025 | 847 | 904 |
| Ligands | 80 | 112 | 109 | 77 |
| RMSD Bonds (Å) | 0.006 | 0.006 | 0.006 | 0.006 |
| RMSD Angles (°) | 0.87 | 0.83 | 0.82 | 0.92 |
| Ramachandran favored (%) | 98.75 | 98.62 | 98.27 | 98.66 |
| Ramachandran allowed (%) | 1.25 | 1.38 | 1.73 | 1.34 |
| Ramachandran outliers (%) | 0 | 0 | 0 | 0 |
| Average B factor ($Å^2$) | 21.82 | 18.33 | 24.84 | 23.51 |
| Protein | 20.05 | 16.39 | 23.11 | 21.60 |
| Solvent | 34.22 | 29.33 | 36.41 | 35.48 |
| Ligands | 33.36 | 20.39 | 31.83 | 35.48 |
| No. TLS groups | 20 | - | 17 | 17 |

[a]Data from the highest-resolution shell is indicated in parentheses.

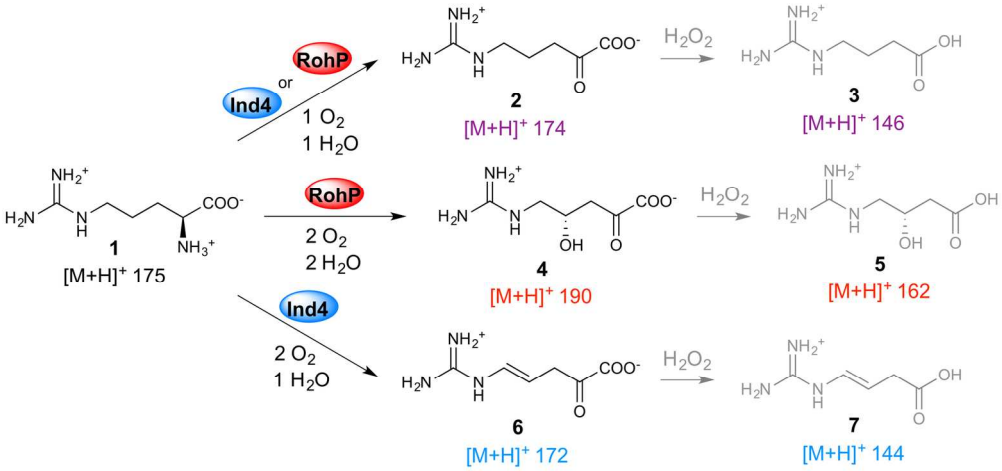


**Figure 1**. Ind4- and RohP-catalyzed reactions. $[M+H]^+$ ions observed from both RohP and Ind4-catalyzed reactions are shown in purple, from only the RohP-catalyzed reactions are in red, and from only the Ind4-catalyzed reaction are in blue. Molecules in gray arise from non-enzymatic reactions with $H_2O_2$.

82x38mm (600 x 600 DPI)

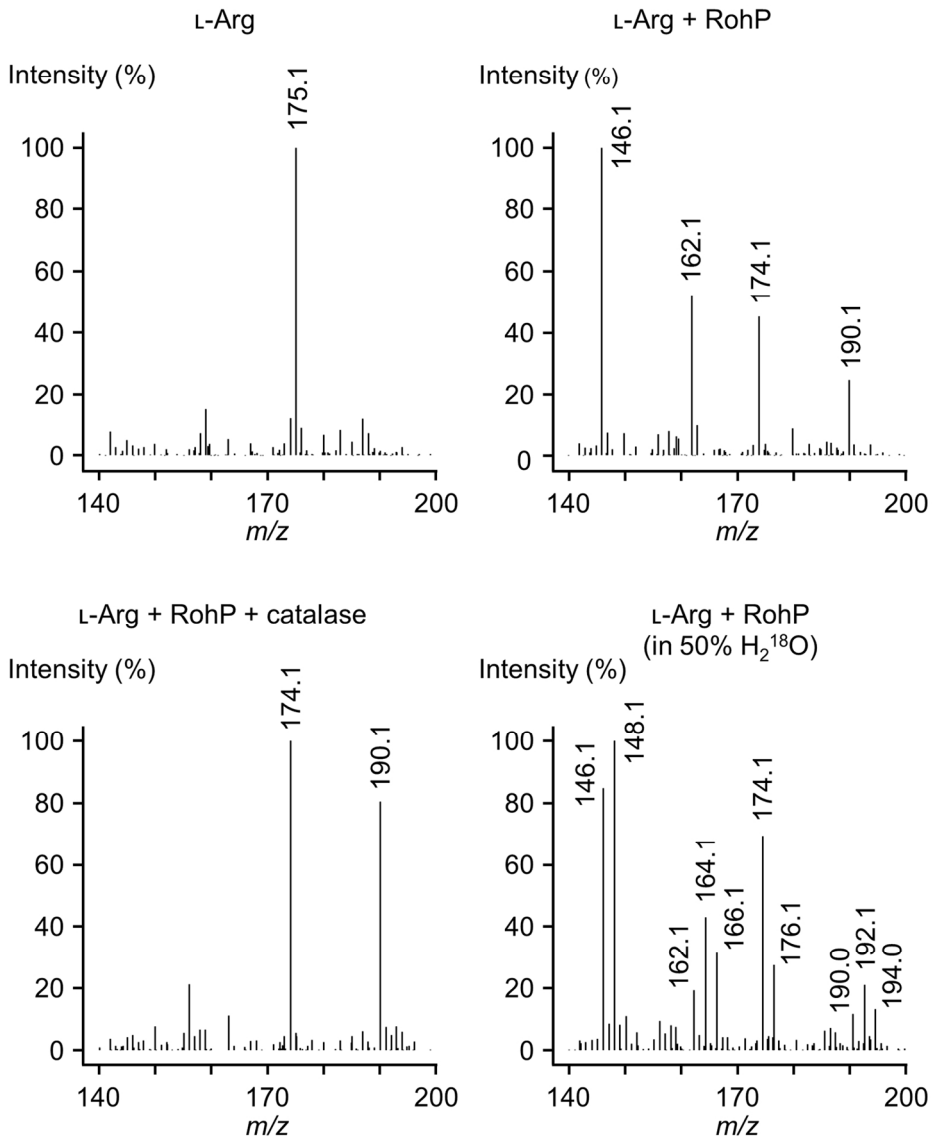


**Figure 2**. RohP-catalyzed oxidation of L-arginine. Liquid chromatography-mass spectrometry analysis of the products of the RohP reaction with L-arginine (L-Arg). The reaction conditions are indicated above each spectrum, and representative integrated total ion chromatograms for each reaction are shown.

140x171mm (300 x 300 DPI)

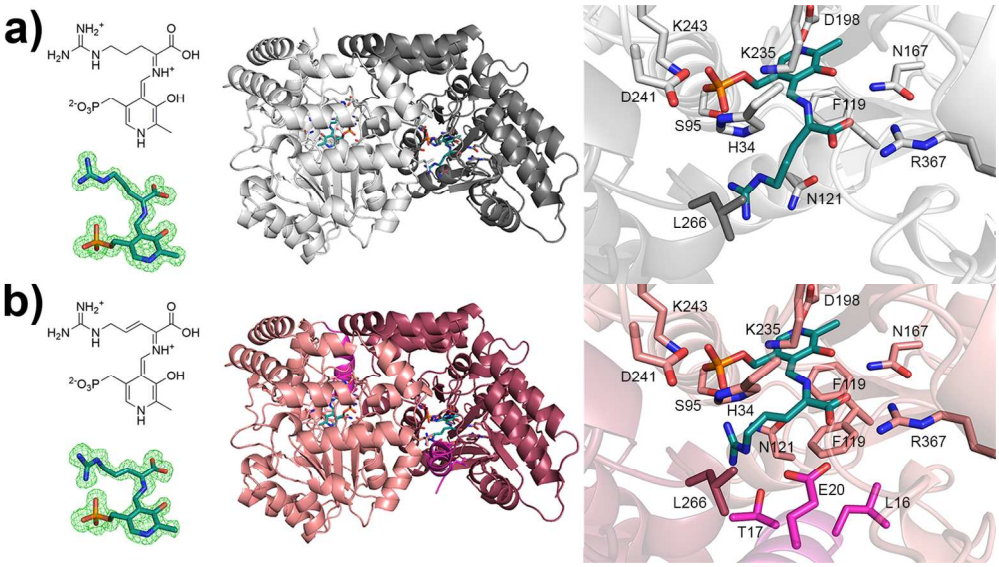


**Figure 3**. Modelling of RohP-quinonoid intermediates. Left Panel: (a) The first quinonoid intermediate (Q1) modelled into the density present in the active site of the first RohP intermediate structure. (b) The second quinonoid intermediate (Q2) with a double bond between arginine Cβ and Cγ modelled into the density present in the active site of the second intermediate structure. Both $F_o$-$F_c$ omit maps are displayed in green and contoured at 3.0 σ. Middle panel: Depicts the entire protein structure as modelled in each structure. The two monomers are indicated with light and dark coloring. The N-terminal helix, absent in holo-RohP, is colored magenta here. Right panel: View of active sites, with nearby conserved residues surrounding the quinonoid intermediates depicted as sticks.

140x77mm (300 x 300 DPI)

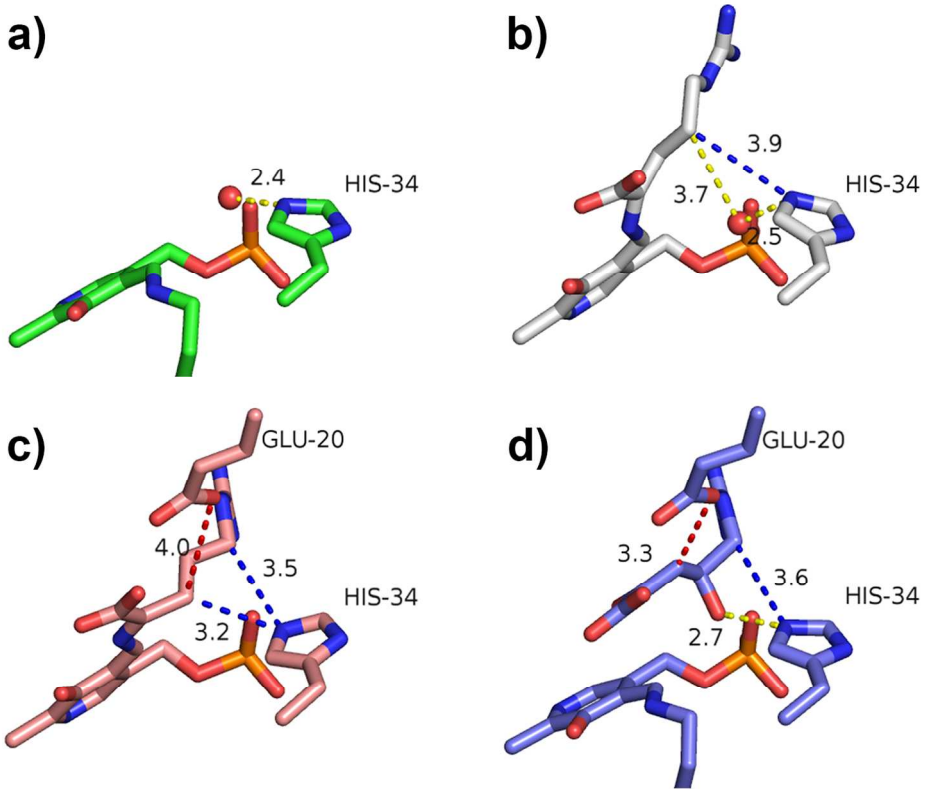


**Figure 4**. Distances between modelled quinonoid intermediates and conserved residues Glu20 and His34 in Chain A of the RohP homodimer. (a) The RohP holoenzyme has only a water molecule (red sphere) positioned 2.4 Å from His34. (b) The N-terminus and Glu20 are absent in the RohP-quinonoid I. His34 is positioned 3.9 Å from the Cγ atom of the bound substrate and 2.5 Å from a water molecule. (c) In the RohP-quinonoid II, the N-terminus is ordered, including Glu20, which is now positioned 4.0 Å from the Cβ of the bound substrate. Furthermore, the new positioning of the amino acid substrate places its Cβ and Cδ atoms 3.2 Å and 3.5 Å, respectively, from His34. No ordered water was present near His34. (d) The product (*S*)-4-hydroxy-2-ketoarginine has its Cβ 3.3 Å from Glu20 and its Cδ 3.6 Å from His34. The 4' hydroxyl group is positioned 2.7 Å from His34.

140x115mm (300 x 300 DPI)

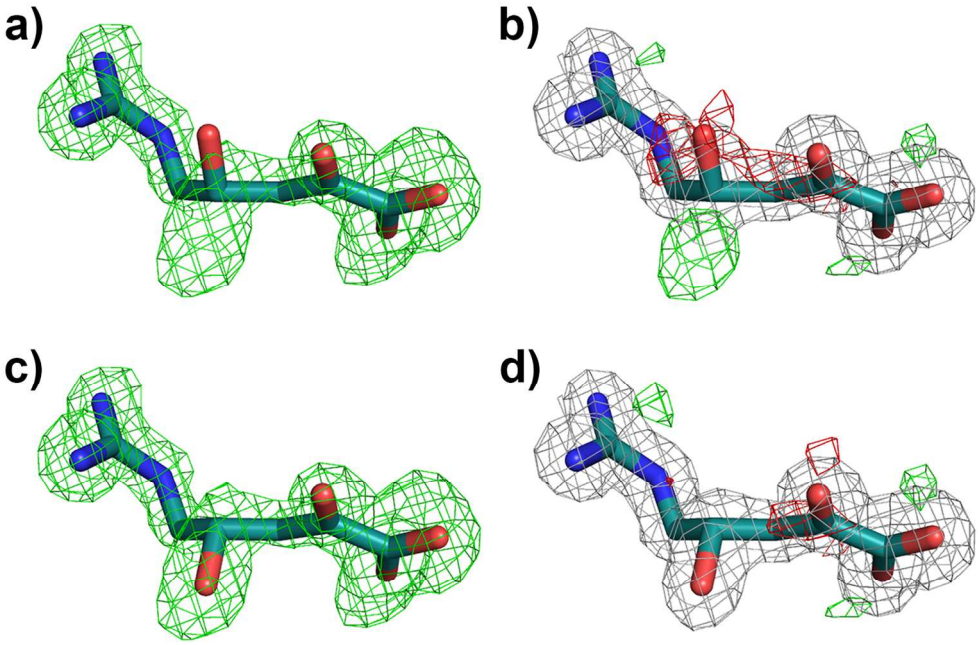


**Figure 5**. Possible stereoisomers of 4-hydroxy-2-ketoarginine. (a) The *R*-enantiomer modelled into $F_o$-$F_c$ omit density present in the active site. (b) The density present around the *R*-enantiomer after refinement using Refmac. (c) The *S*-enantiomer modelled into $F_o$-$F_c$ omit density present in the active site. (d) The density present around the *S*-enantiomer after refinement using Refmac. The $F_o$-$F_c$ maps are contoured at 3.0 σ with positive and negative density indicated as green and red, respectively. The $2F_o$-$F_c$ maps are contoured at 1.0 σ in gray. Ligands were built using eLBOW in the Phenix software suite.

140x95mm (300 x 300 DPI)

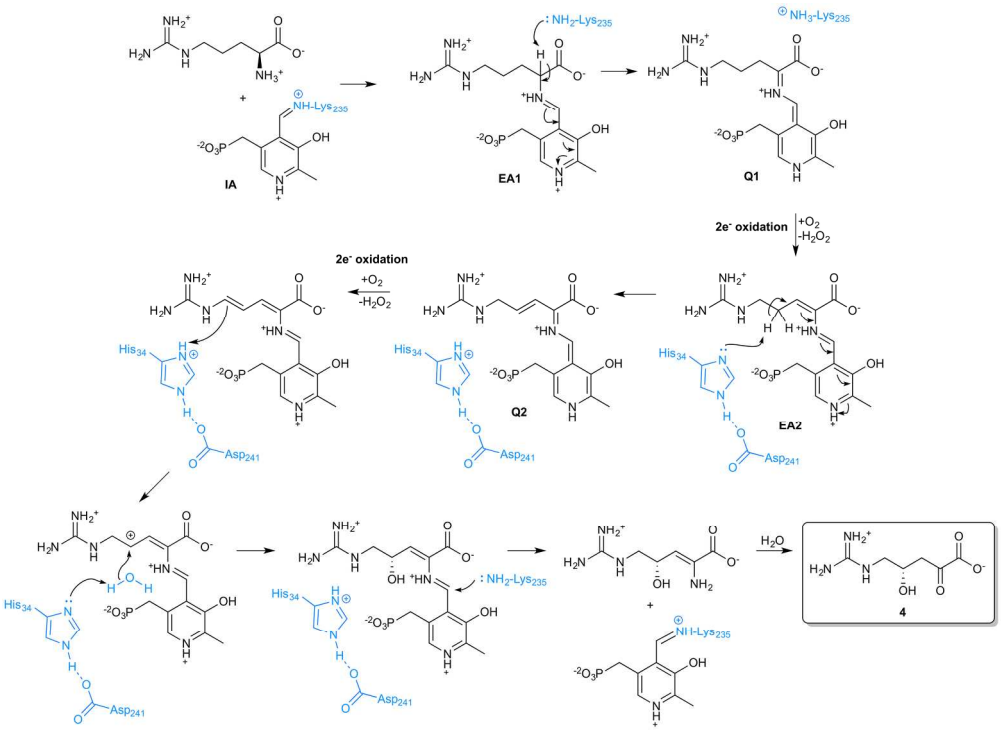


**Figure 6**. Proposed mechanism of the RohP catalyzed reaction to give **4**.

102x74mm (600 x 600 DPI)